ORIGINAL ARTICLE

Environmental fluid mechanics of minimum energy loss weirs: hydrodynamics and self-aeration at Chinchilla MEL weir during the November–December 2021 flood event

Hubert Chanson[1] (ORCID) · Colin J. Apelt[1]

Abstract

During the recent decades, a number of overflow embankment protection systems were implemented. One design is the Minimum Energy Loss (MEL) weir, developed to pass large flood events with minimum energy loss and low erosion. Several MEL weirs have successfully operated for decades in Australian catchments affected by heavy tropical and sub-tropical rainfalls with very flat gradients. Their historical performances are discussed and confirmed the design capability to pass large floods with small afflux and very small energy loss and little environmental impact including no significant erosion at the abutments. During a major flood, visual and quantitative observations were undertaken at the Chinchilla MEL weir. On the smooth converging chute, the observations showed that the inception of self-aeration was a three-dimensional process with a gradual change in free-surface roughness, from a smooth glassy free-surface to a very-rough choppy surface. An optical technique (OF) was implemented to derive the contour maps of surface velocities based upon video movies taken from a sturdy tripod. The self-aerated flow velocity data were close to the backwater equation in the self-aerated region, while highlighting regions of high- and low-velocities across the chute. The OF data showed large streamwise surface velocity fluctuations in the aerated flow region, consistent with the broad literature on self-aerated flow measurements. The ratio of transverse to streamwise surface turbulence intensity indicated a strong anisotropy of the free-surface turbulence.

Highlights

- Minimum energy loss (MEL) weirs were developed for river catchment with heavy rainfall and very flat gradient.
- Field observations were performed at the Chinchilla MEL weir spillway in late 2021 during a major flood.

✉ Hubert Chanson
h.chanson@uq.edu.au

Colin J. Apelt
colin_apelt@bigpond.com

[1] School of Civil Engineering, The University of Queensland, Brisbane, QLD 4072, Australia

- Surface velocity data showed large transverse difference in longitudinal surface velocities across the chute

1 Introduction

During the recent decades, a number of overflow embankment protection systems were developed and implemented [18, 27]. These include the earth dam spillway with precast concrete blocks [28, 48], some Roller Compacted Concrete (RCC) protection of the downstream slope of embankment dams [13, 44] and the Minimum Energy Loss (MEL) weir [43]. The MEL weir structures are designed to pass large flood events with minimum energy loss and low erosion, and several MEL weirs have successfully operated for decades in Australian catchments affected by heavy tropical and sub-tropical rainfalls with very flat gradients, i.e. $S_o \sim 0.1\%$ [43, 55].

In most overflow spillways, the upstream flow region is brown and non-aerated, and a strong air–water mixture develops downstream of the onset region of air entrainment [30, 37]. At the upstream end of the spillway, the flow is accelerated in a relatively smooth manner [29, 36]. A turbulent boundary layer develops along the invert from the upstream end [32, 34]. On a steep overflow spillway, the inception of free-surface aeration typically occurs when the outer edge of the bottom boundary layer starts to interfere with the water surface [31, 36, 50]. The interactions between boundary layer turbulence and free-surface can be explosive accompanied by strong projections of air–water packets [16, 21, 57]. In contrast, on a flat chute, the onset region exhibits a free surface with the gradual development of small ripple and surface instabilities, and the water surface tends to present a choppy appearance when self-aeration starts to occur [11, 12, 46]. Levi [40, 41] and Anwar [1] argued that the inception conditions then combine the effects of longitudinal vortices' breakdown and of gravity waves produced by boundary irregularities and roughness. Recently, Toro et al. [54] and Chanson [19, 21] demonstrated that the two theories are not exclusive using two different approaches. That is, three-dimensional Computational Fluid Dynamics (CFD) computations [54] and detailed prototype observations [19, 21] respectively. The inception region of free-surface aeration is illustrated on two prototype spillways in Fig. 1, using high-shutter speed (1/8000 s) photographs of the onset region in relatively steep and flat overflow chutes, i.e. Figure 1A, B respectively. The location of both structures is shown in Fig. 2.

To date, the literature on prototype spillway operation, including minimum energy loss (MEL) weirs, is very limited, with negligible quantitative field data. Herein, a series of field observations was conducted in a large protype MEL weir during a major flood event in late 2021. The contribution first aims to describe the process that led to the MEL weir design concept and to review the performance of MEL weirs taking into account recent observations of the effects of major flood events on the MEL weir at Chinchilla. The latter is complemented by an unique series of field observations including detailed quantitative measurements performed in terms of the surface velocity field in the high-speed, high-Reynolds-number overflow. Some key features of the inception region of free-surface aeration were described, showing the onset of air entrapment being a complicated

(A) Inception region on a steep chute: Hinze Dam Stage 3 spillway (Australia) on 24 March 2021 (θ = 45.9° [at inception], Re = 5.6×10^7, Shutter speed: 1/8,000 s) - Top: view from downstream of the inception region; Bottom: view from upstream of the inception - Arrows indicate the main flow direction

Fig. 1 Onset of self-aeration on overflow spillways

(B) Inception region on a flat chute: Chinchilla MEL weir (Australia) on 27 November 2021 ($\theta = 11.3°$,

Re = 2.3×10^6 [at inception], Shutter speed: 1/8,000) - Top: General view from the right bank; Bottom:

details of inception region from the previous photograph - Arrows indicate the main flow direction

Fig. 1 (continued)

process, while the surface velocity field differed from the assumed one-dimensional flow (1D) pattern.

2 Design development and concepts of minimum energy loss weir

2.1 Presentation

The Minimum Energy Loss (MEL) weir design approach was developed in response to the failure to achieve a satisfactory design of a "conventional" weir for a site on Sandy Creek near Clermont, Queensland (QLD), Northern Autralia. Through physical model tests of many conventional weirs, late Professor Gordon Reinecke ("Mac") McKay (1913–1989) progressively refined the weir design. In essence, his strategy had as its main features: (i) arrange the level of the crest in several steps, rising progressively on each side from the central section in order to reduce the difference between the flow distribution over the weir and that in the natural stream and thereby reduce the potential for bank erosion; (ii) reduce as much as possible the afflux across the weir when the upstream flood level overtopped the banks in order to reduce the potential scour at the abutments: (iii) design adequate

Fig. 2 Map of Australia including the location of the Sandy Creek weir, Clermont and Chinchilla weir, and Hinze dam in Queensland

scour protection for the embankments to prevent scour there. An example of such a design is the weir on Wararba Creek near Caboolture, Queensland, Eastern Australia (Fig. 3). However, eventually it proved impossible to develop a satisfactory design based on these principles for the site on Sandy Creek, despite a large number of attempts. The competing requirements for this weir and for many others constructed in streams with erodible banks are: (1) maximum in-stream storage, (2) protection against erosion of the stream banks at the abutments of the weir and downstream and (3) no increase in the frequency of out-of-bank flooding. The conventional type of weir caused excessive afflux and over-bank flow and massive erosion of the alluvial banks at the abutments and downstream, even for flows considerably less than the design flow. When Apelt [4] was invited to observe the performance of the last of these unsatisfactory model tests, it was clear that the weir was causing too much constriction of the flow with large energy losses. He noted that the flow over the weir was analogous to that past an orifice plate in a pipe and suggested an approach analogous to a Venturi tube. The idea was to minimise the energy loss across the structure by using a more streamlined geometry everywhere and a gradual expansion downstream to recover as much as possible of the kinetic energy of the flow at the weir crest. A large number of trials finally produced a satisfactory design for the site on Sandy Creek, Clermont and the first MEL weir was built there in 1962 (Fig. 4) [4].

The essential principles of the approach, described as the Minimum Energy Loss (MEL) weir design, are simple: (i) the crest is made long enough to pass the bank-full flow at critical conditions with the simplifying assumption there is no energy loss and therefore no change in the upstream water level; (ii) the weir crest in plan is a circular arc of the length required by the first principle and concave downstream in order to converge the flow horizontally towards the centre of the stream after it has passed the crest; (iii) the faces of the weir must have relatively flat slopes to reduce energy losses by avoiding rapid lateral

Fig. 3 In-stream weir on Wararba Creek weir near Caboolture (Australia) in the 1960s (Photographer Roy Dobson. Image courtesy of Moreton Bay Regional Council, reference number CLPC-P2299)

convergence horizontally and expansion of the flow in the vertical plane as it passes over the weir; the downstream face has a much flatter slope than does the upstream face. In order to satisfy the first two principles, the upper levels of the banks immediately upstream

Fig. 4 Sandy Creek MEL weir at Clermont—Top: discharging a small flow about 142 m3/s (Collection of late Professor G.R. McKay); Bottom: large flood event on 3 August 1993 (Courtesy of A.J. Holmes)
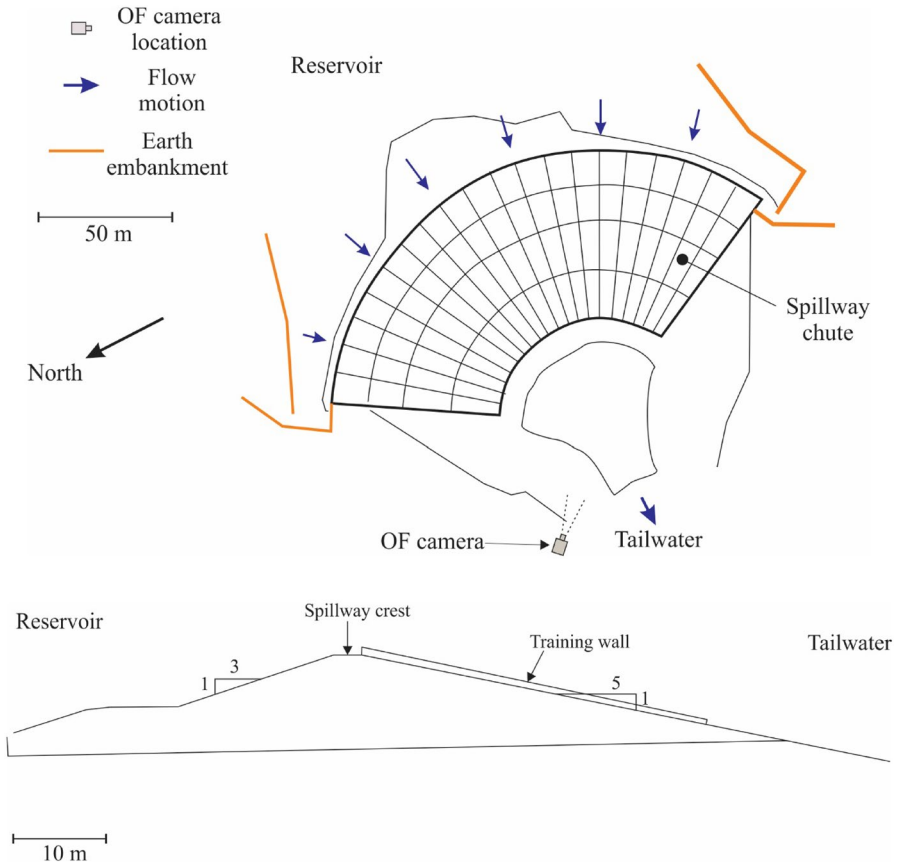
Fig. 5 Plan view and cross-section of Chinchilla MEL weir (redrawn after [55])

from the weir crest are excavated sufficiently to provide for efficient flow normal to the crest, uniformly distributed along its full length. Figure 5, based on the design drawings of the Chinchilla MEL weir, illustrates these principles.

2.2 Discussion

The MEL weir design presents a number of advantages. The weir passes the bank-full flow with little afflux. The term "afflux" is used here to describe the increase in the actual water level upstream from the weir above the undisturbed water level that would have existed in the absence of the weir (see discussion Sect. 2.3). The simple design approach implies that no energy loss occurs as the flow approaches and passes over the weir crest. Clearly, this is an oversimplification and, inevitably, some energy loss occurs though it is much smaller than that for a conventional weir. Consequently, the bank-full flow with the weir in place will be slightly smaller than for the undisturbed stream. As a consequence of the small energy loss, the crest level of the MEL weir can be much higher than would be feasible for a conventional weir for the same design flow and the water storage capacity is much increased. The horizontal convergence of the flow downstream from the crest results in a

flow distribution much closer to that of the natural stream than is achievable with a conventional weir and the potential for bank erosion is much reduced.

There are however a number of disadvantages. Because of the flatter cross-sectional shape, the construction of a MEL weir involves a much larger volume of material than is needed for a conventional concrete gravity weir. Typically, the approach has been to construct the weir as a compacted earth embankment covered everywhere by concrete slabs with provision for drainage to relieve any water pressure that develops in the embankment. Inevitably, there is risk of damage should a significant flow occur during construction. The MEL weir on Sandy Creek at Clermont was built in 1962. When it was nearly completed a minor flood overtopped it and caused considerable damage. The weir was completed at the next attempt. The construction of the MEL weir on the Condamine River at Chinchilla began in late 1972 but was interrupted by a large flood in October 1972 that caused extensive damage when the weir was nearly completed. Unfortunately, when the renewed construction was almost finished, another flood in July 1973 caused extensive damage. Eventually the weir was completed successfully in December 1973 [55].

Whether an MEL weir is appropriate for a particular site will depend on the design criteria and on the relative costs—that must include some insurance against possible damage during construction if there is a risk of flooding.

2.3 Historical performance of MEL weirs

The weir at Clermont has been in operation for about 60 years, that at Chinchilla for nearly 50 years and a review of their performance is instructive. The significant criteria in such review are whether there have been issues concerning erosion and the hydraulic performance.

The MEL weir on Sandy Creek, Clermont was designed for a design head of 2.9 m. McKay [43] reported that the MEL weir "has been overflowed many times, but the size of the maximum flow is not known. No scour or erosion has taken place downstream". In Apelt [2], J.D. Turnbull reported that "no further problems have been reported from the weir" since completion of construction. The weir is still in use as an emergency water supply [14].

The Chinchilla minimum energy loss weir (QLD, Australia) (Figs. 1B, 5) is located in the Western Downs, along the Condamine River to provide both town and irrigation water supply [49]. The longitudinal river bed slope is $S_o = 0.215\%$ in average between Brigalow and Chinchilla weir. Completed in 1973, the weir provides irrigation water, and it is listed as a "large dam". With a catchment area of 19,192 km^2, the weir is a 14 m high earth fill embankment with a 410 m long dam crest including abutments. The overflow spillway (Fig. 1B) has a design capacity is of 850 m^3/s corresponding to bank full at a design head 1.83 m. The spillway system consists of a broad crest that is 214 m long, followed by a smooth converging chute with a 1 V:5H slope. There is no stilling basin. After completion, grass was planted in the top soil and protective mesh that had been placed on the subsidiary earth embankments on each bank. Before this had time to grow, the weir was subjected to a major out-of-bank flood of order 1,130 m^3/s, one of the highest on record, and that overtopped the embankments [55]. At the peak of the flood, it was difficult to see where the weir was, because it was completely drowned out. As the flood receded, it was wonderful to see the structure emerge from the flood waters relatively unscathed. The top soil and grass planted over the plastic mesh and gravel on the top of these embankments were washed away for the most part, but the mesh

Table 1 Maximum water elevation observations during major flood events at Chinchilla weir tailwater and headwater (QLD, Australia)

Date of peak of flood event	Time of flood peak	Tailwater (m AHD)	Headwater (m AHD)	Afflux (m)	Q (m³/s)
February 1942	–	296.76	–	–	–
January 1956	–	296.69	–	–	–
February 1976	–	296.72	–	–	–
May 1983	–	296.33	–	–	–
May 1996	–	296.14	–	–	–
January2004	–	290.23	–	–	–
December 2010	–	298.20	–	–	–
January 2011	–	297.21	–	–	–
February 2013	–	295.23	–	–	–
5 December 2021	11:20	295.54	298.77	3.23	1,918
4 March 2022	00:00	294.25	297.58	3.33	907
1 April 2022	07:00	295.27	298.48	3.21	1,649
11 April 2022	06:00	293.77	297.07	3.30	558
20 May 2022	08:10	294.33	297.69	3.36	990

AHD Australian height datum. Q: spillway chute discharge; Data: TMR 1969, BOM 2017, Present study. (–): data not available

held and the damage was minor. The soil and grass were replaced and the grass became well established before the next flood [2]. Since the weir's completion, the Condamine River at Chinchilla has carried a large number of floods in that period, many of them being major out-of-bank floods. Between 1973 and 2022, the weir was overtopped by a number of large flood events, including events larger than the design flow (Table 1). The weir operated safely and properly, and inspections after the flood showed no damage. The first author has inspected the weir several times and found no evidence of erosion. Most recently he visited soon after a major out-of-bank flood in November/December 2021. The flood level had risen to at least 2.5 m above the right bank at the carpark, and no erosion had occurred.

The Chinchilla MEL weir was designed to give no afflux at bank full flow, 850 m³/s, when the head over the weir is only 1.83 m, [55]. Although the design of the weir itself was based on the assumption that no energy losses occurred, "the level of the supplementary embankments was determined from theory and the model as the lowest head water level at which there would be an afflux of less than one foot (300 mm)" [55]. The term "afflux" was used here to describe the increase in the actual water level upstream from the weir above the undisturbed water level that would have existed in the absence of the weir. Implicit in this definition is the assumption of steady flow in a uniform channel. During the major flood in 1973 of order 1,130 m³/s, the measured afflux at the bank full flow was only 100 mm, i.e. the head over the crest was 1.93 m, only slightly larger than the simple design assumption [55]. It was not stated how this was measured—it would be a very difficult procedure during a major flood. Elsewhere, the cited authors stated that, for the same conditions, the measured afflux was approximately six inches (0.150 m) compared with the model estimate of over one foot (0.305 m).

With the uncertainty about the stated magnitudes of afflux based on observation during the flood, it is thought that the most likely magnitude is that measured on the

model—"over" 300 mm. Photographs of the model [2, 5] showed that this measurement was made just upstream from the weir. In contrast to the usage here, the usual meaning given to afflux is the difference between the observed headwater and tailwater elevations at a structure such as a weir [3, 15]. This will be discussed further in the context of flood levels recorded during a major flood in November/December 2021.

The historical performance of both MEL weirs discussed has shown that, even during large out-of-bank floods, they cause no significant erosion at their abutments or down-stream—the regions that are most at risk and require extensive protection for conventional weirs. There is evidence that they do cause some small increase in flood levels upstream during what would have been a bank-full flood, but it is difficult to assess the magnitude of this. Overall, the MEL weirs have much less environmental impact than conventional weirs.

3 Chinchilla weir field study and methodology

3.1 Presentation and instrumentation

The Chinchilla MEL weir (QLD, Australia) is located on the Condamine River, on the northern part of the Murray-Darling basin (Fig. 2). The catchment area is 19,192 km^2. The weir experienced a large flood event in Nov./Dec. 2021 and field observations took place. The maximum tailwater elevation and afflux at the peak of the 2021 flood event are reported in Table 1 and compared with several documented major floods, including several major floods in 2022 (Table 1).

The water discharge was deduced from the measured reservoir elevation, using the predicted discharge coefficient, based upon the drawings as constructed (Fig. 5) [33]. Visual, photographic and cinematographic records were undertaken from the right bank of the spillway and from the right river bank downstream of the spillway toe. Figures 1B and 6 present hand-held photographs taken from several locations. The observations were conducted using three dSLR Pentax™ cameras with sensor resolutions between 12 and 24 Mpx, a digital camera Sony™ RC100VA and an iPhone XI. The dSLR cameras were equipped with full-frame prime lenses producing photographs and movies with negligible barrel distortion. The dSLR camera movies were recorded in high definition (1920×1080 px) at 30 fps and 60 fps.

The analyses of surface features were conducted using both high-shutter speed photographs and video movies. For all the cases, the tracking and measurements of the water surface features were conducted manually to guarantee the best quality control, owing to the complexity of the prototype flow's turbulent motion, characterised by very rapid and unpredictable changes with time and space. Further, a number of movies were taken from downstream and analysed using an optical flow (OF) technique, with the camera fixed on a sturdy professional-grade tripod. The study area covered by the non-intrusive optical measurements of surface velocity was restricted to the left spillway bay, because of optical access limitations. The Optical Flow (OF) is a set of tools, detecting the flow motion between consecutive frames based upon brightness intensity gradients [9, 59]. In the current study, Farnebäck's [26] OF technique was applied to calculate the surface velocity field based upon movies recorded from a camera fixed on a sturdy tripod. The Farnebäck OF technique was applied with OF parameters previously validated in laboratory for surface velocity field [6] and used for the Hinze Dam prototype spillway data sets [20]. It is

(A) Upstream flow viewed from downstream on 27 November 2021 (Shutter speed: 1/8,000 s) - View

of the left spillway chute from the OF camera shown in Figure 5A
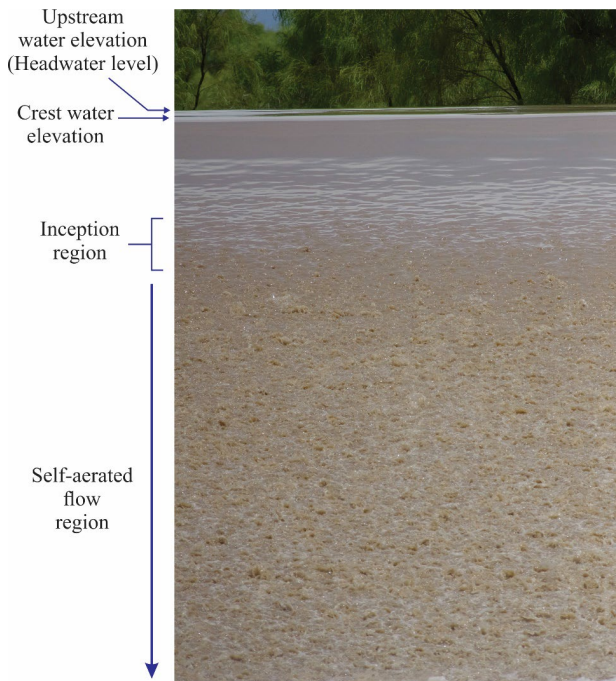
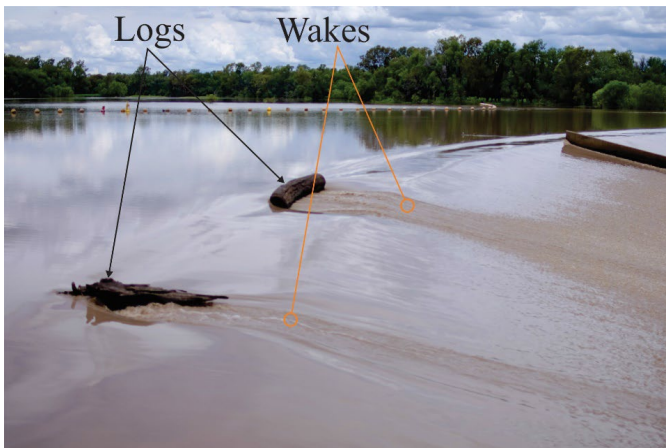(B) Timber logs blocked at the spillway crest on 27 November 2021 (Shutter speed: 1/8,000 s)

Fig. 6 Photographs of the spillway operation at Chinchilla MEL weir (QLD, Australia) during the major flood in Nov./Dec. 2021

acknowledged that the OF calculations were not truly 'calibrated' owing to the significant number of intrinsic difficulties with field observations during flood events, including uncontrolled optical conditions [19, 20]. Since the camera field of view was perpendicular to the spillway chute, the raw data included the vertical and horizontal surface velocity components recorded at various vertical elevations. The streamwise surface velocity was deduced from the vertical surface velocity component and invert slope based upon geometric considerations, assuming a two-dimensional flow.

3.2 Prototype flow conditions

In November 2021, more than 100 mm of rainfall was recorded in the Condamine River catchment area upstream of Chinchilla, mostly from mid-November.[1] The Chinchilla weir overflowed for more than one month, with the peak headwater observed on 5 December 2021 morning. Observations of overflow discharges are presented in Fig. 7A. For seven days, the spillway discharged a flow rate greater than the bank full design discharge, with a peak flow about 1,930 m^3/s corresponding to 2.3 times the design discharge. Note that the inspection on 15 December 2021 confirmed that the abutments were overtopped by nearly 3 m of water at the peak of the flood, without damage.

The Chinchilla weir overflow was documented on 27 November 2021 and 15 December 2021. The first data set was obtained at the start of the flood event, while the second took place after the peak of the flood (Fig. 7). The flow conditions at the time of observations are detailed in Table 2. Note that the weir overflow could not be witnessed at the peak of the flood by the authors, because the access road become submerged when the tailwater elevation exceeds about 290–291 m AHD. The afflux, difference between recorded High Water Rating Level (HWRL) and Tailwater Rating Level (TWRL), was 3.23 m at the peak of the flood event (Fig. 7B), which was somewhat consistent with some photographic observation by a local on 5 December 2021 morning. The maximum tailwater elevation and afflux during the 2021 flood event is compared with several documented major floods, including several major floods in 2022 in Table 1.

3.3 Discussion on the afflux

The differences between the magnitudes of the afflux given in Table 1 and those reported in the preceding section on historical performance are due, at least partly, to the difference between the meaning of the term implicit in the discussion of the afflux reported to have been observed during the major flood in 1973 [55] and its meaning as specified for Table 1. Clearly, the assumption of steady flow in a uniform channel, implicit in the use of the term in Turnbull and McKay [55] is not valid for a time varying flood event in a real river— the Condamine River is very nonuniform in cross - section. In Table 1, the headwater and tailwater elevations are those observed at the respective flood gauges maintained by the Australian Bureau of Meteorology. These are some distance from the weir and part of the afflux reported in Table 1 would be due to the flood gradient at the time. Further, it is not known whether all of the flow diverted from the river upstream from the weir during overbank stages returns to the main channel upstream from the tailwater gauge. Nevertheless,

---

[1] As an illustration, the Warwick Alert station recorded 206 mm of rainfall in November 2021, which what the highest monthly record for the period 1995–2021 (BOM 2022, Monthly rainfall). The station is located in the upper Condamine catchment, 220 km South-west of Chinchilla.

(A) Water discharge over the spillway excluding the abutment overflows
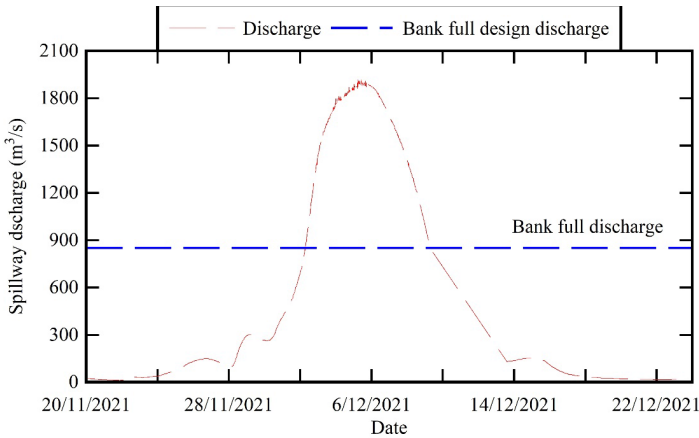
(B) Measured headwater levels, tailwater levels and afflux - the afflux being defined as the difference between the headwater level (H.W.L) and tailwater level (T.W.L.)
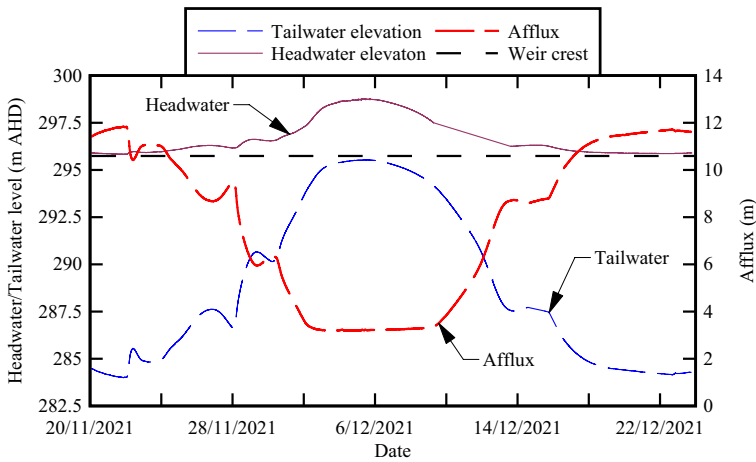

Fig. 7 Spillway operation at Chinchilla MEL weir (QLD, Australia) during the major flood in Nov./Dec. 2021: water discharge over the spillway and afflux

Table 2 Observations of Chinchilla MEL weir (QLD, Australia) spillway operation during the major flood in Nov./Dec. 2021

Date	Time	Headwater (m AHD)	Tailwater (m AHD)	Q (m³/s)	Re (at spillway crest)
27 November 2021	12:45–13:20	296.23	287.20	121	2.3×10^6
15 December 2021	12:30–13:30	296.29	287.52	144	2.7×10^6

AHD Australian height datum

Table 3 Location and depth at the onset of free-surface aeration at Chinchilla MEL weir (QLD, Australia) during the major flood in Nov./Dec. 2021

Date	Time	Q (m³/s)	Head above crest (m)	x_I[a] (m)	d_I[b] (m)	x_I predicted[c] (m)	d_I predicted[c] (m)
27 November 2021	12:45–13:20	121	0.49	7.5	0.11	10.2	0.10
15 December 2021	12:30–13:30	144	0.55	13.4	0.12	11.6	0.12

[a]Statistical median value of photographic and cinematographic data

[b]Water depth estimate deduced from present backwater calculation

[c]Correlations of Cain and Wood [10]

it is clear that the increase in flood levels upstream due to the weir, while small, are larger than those implicit in its design, but it is not possible to estimate the magnitude of this difference from the available information.

4 Basic flow observations and self-aeration

On both occasions (Table 2), the approach flow was very smooth, and this was confirmed by aerial footages on 21 December 2018 and on 3 December 2021. The reservoir flow converged smoothly towards the weir crest and the water surface was waveless and almost still. On both 27 November 2021 and 15 December 2021, the flow was critical at the spillway crest which acted as a broad-crested weir, with a ratio of crest length to upstream head over crest of 6.2 and 5.54 respectively. The smooth change on water surface elevation between the upstream reservoir and spillway crest was nicely documented with photographs (Fig. 6A). Immediately downstream of the broad-crest, the water surface was smooth and glassy (Figs. 1B, 6). On 27 November 2021, a few logs were trapped at the crest, and their wake was clearly seen at the surface of the non-aerated flow. Further downstream, the wake progressively disappeared in the self-aerated air–water flow region (Fig. 6B).

As the flow accelerated down the smooth converging chute, the glassy free-surface became rough and choppy, before becoming self-aerated, i.e. the inception region. The inception region showed a progressive transition of the surface roughness, from a smooth glassy surface to a rough, coarse-sand-paper-like appearance and further downstream to a very-rough choppy surface (Fig. 6). The self-aerated region presented a beige colour, evidence of a three-phase air–water sediment motion. Such an observation was well-documented visually on both 27 November and 15 December 2021, as well as during an earlier overflow on 8 November 1997 [53].

The average location x_I of the inception region of self-aeration was recorded during both overflows, and the data are reported in Table 3 (column 5). The corresponding water depth d_I was deduced for the backwater calculations (Table 3, column 6). The observations are compared to the correlations of Cain and Wood [10] for a smooth prismatic channel, assuming $k_s = 1$ mm as used in the backwater calculations (see below). The comparative results (Table 3) showed a close agreement in terms of the water depth at inception, while the observed location data presented more scatter,

possibly caused by the wide spread of the inception region, while the flow convergence was expected to induce a slower growth in bottom boundary layer compared to prismatic chutes. Physically, the converging chute geometry has two major effects on the free-surface aeration inception conditions. First, the chute convergence yields a greater water depth at a given vertical elevation for a given discharge than in absence of convergence, based upon conservation of mass since the free-stream velocity is unchanged, Second, the contraction of the chute affects the turbulent boundary layer development, as predicted by the von Karman momentum integral equation [17, 42]. The former might have a more sizeable impact, leading to a further downstream self-aeration inception region location.

The video movies further showed the occurrence of some form of two-dimensional roll waves in the self-aerated flow region. The phenomenon was clearly seen on 27 November 2021, and less visible on 15 December 2021. Although the same camera system (camera body and lens) was used on both occasions, the difference might be linked to differences in light conditions as well as slightly different water discharges. For completeness, the quasi-two-dimensional roll wave patterns was not visually seen in-situ, but it was clearly evidenced during the movie replay, as well as in the OF data. For both flow conditions, the instability criteria of Keulegan and Patterson [35] was fulfilled [25]. The Vedernikov number [24, 47] was greater than unity at the chute toe, being equal to 2.5 and 3.7 on 27 November 2021 and 15 December 2021 respectively. The observed longitudinal (roll) wave length was $\lambda/d \approx 18.4$ and 19 on 27 November 2021 and 15 December 2021 respectively, and the amplitude of the longitudinal oscillations of the time-averaged streamwise surface velocity was about $\Delta V_s/(g \times d)^{1/2} \approx 0.11$ and 0.26 respectively, with d and V the local water depth and depth-averaged velocity. Dressler's [25] calculations of the roll wave speed yielded a celerity about equal to the chute toe velocity, implying some quasi-stationary roller waves, that would be consistent with the interpretation of the video movies for both flow conditions.

At the toe of the spillway chute, the high-velocity self-aerated flow impinged into the tailwater and a hydraulic jump formed. The jump was stationary and very stable, located on the underwater sloping chute on both days. The position of the jump was controlled by the tailwater conditions and the very-flat Condamine River channel bed slope downstream of Chinchilla. The jump roller was highly turbulent and fluctuating about its mean position. Both visual and video movie observations indicated strong three-dimensional large-scale vortices in the roller. The interactions of these large turbulent structures with the roller free-surface created large scars and surface features, with length-scales comparable to the roller height.

5 Surface velocity observations

5.1 Presentation

Based upon the video movies of the left chute centreline, taken from downstream, the surface velocity field was measured in the plane parallel to the invert using the optical flow (OF) technique. Both the streamwise velocity V_s and transverse velocity V_t components were extracted. First, the present data provided physically meaningless results in the upstream non-aerated flow region. This was most likely caused by the shiny surface glare, seen in Figs. 1B and 6, upstream of the inception region. Second, physically meaningful

surface velocity results were obtained in the self-aerated flow region and are presented below. This finding differed from the OF observations at the Hinze Dam spillway [19, 20] and are discussed later.

For the left spillway section, the time-averaged centreline OF surface velocities were compared to the ideal fluid flow theory and to the backwater equation. On an uncontrolled chute spillway, the flow is accelerated by the gravity force component in the flow direction. The ideal velocity V_{max} at a sampling location on the chute is derived from the Bernoulli principle:

$$V_{max} = \sqrt{2 \times g \times (H_1 - d \times \cos \theta)} \tag{1}$$

where H_1 is the upstream total head above the sampling point, θ is the channel slope and d is the water depth [15], pp. 407 & 486). For a steady non-uniform real fluid flow, the differential form of the energy equation is called the backwater calculations developed assuming that the flow is gradually varied. For a rectangular channel of non-constant slope and width, the backwater equation yields [15], pp. 377–381):

$$\frac{\partial d}{\partial x} \times (\cos \theta - Fr^2) = -\frac{\partial z_o}{\partial x} - S_f + d \times \sin \theta \times \frac{\partial \theta}{\partial x} + Fr^2 \times \frac{d}{B} \times \frac{\partial B}{\partial x} \tag{2}$$

$$Fr = \frac{Q}{\sqrt{g \times d^3 \times B}} \tag{3}$$

with S_f the friction slope, and B the free-surface width. At Chinchilla MEL weir, the channel cross-section is rectangular and the chute has a constant slope ($\theta = 11.31°$) with a reducing width. Then, the backwater equation becomes:

$$\frac{\partial d}{\partial x} \times (\cos \theta - Fr^2) = -\frac{\partial z_o}{\partial x} - S_f + Fr^2 \times \frac{d}{B} \times \frac{\partial B}{\partial x} \tag{4}$$

with $\cos\theta = 0.9806$, $\sin\theta = 0.196$, and $\partial B/\partial x = -2.1805$ at the Chinchilla MEL weir.

The surface velocity data showed a relatively close agreement between the time-averaged streamwise OF surface velocity and the backwater-calculated velocity downstream of the onset region, both qualitatively and quantitatively (Fig. 8). Figure 8 presents some typical comparisons in terms of streamwise surface velocity component V_s, with each graph corresponding to one movie. In Fig. 8, the ideal fluid flow estimates are shown with a solid green curve and the backwater calculations are the dashed red curve. For completeness, the streamwise surface velocity standard deviation v_s' and transverse surface velocity standard deviation v_t' are added in Fig. 8. In Fig. 8, the vertical axis is the vertical elevation in m AHD, where AHD stands for Australian Height Datum, and the horizontal axis is the surface velocity data in a dimensional form.

The time-averaged OF surface velocity data presented a number of key features. Firstly, the time-averaged longitudinal velocity component increased with decreasing vertical elevation, as it would be physically expected (Fig. 8). Secondly, the longitudinal velocity data showed some poor agreement with ideal fluid velocity estimates in the developing non-aerated flow region. For $z_o > 294$ m AHD, the poor results were caused by the water surface reflections, seen in Figs. 1A and 6, preventing the OF technique to track the flow motion based upon the brightness intensity gradient. Thirdly, the time-averaged OF velocity data agreed relatively well with the backwater calculations developed for the converging chute (see above) and valid in the fully-developed self-aerated flow region.

(A) On 27 November 2022 (Q = 121 m³/s)
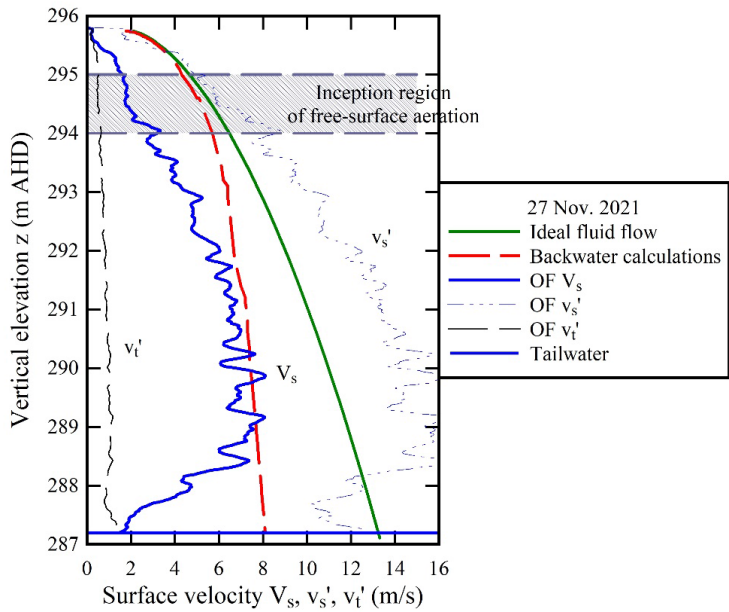
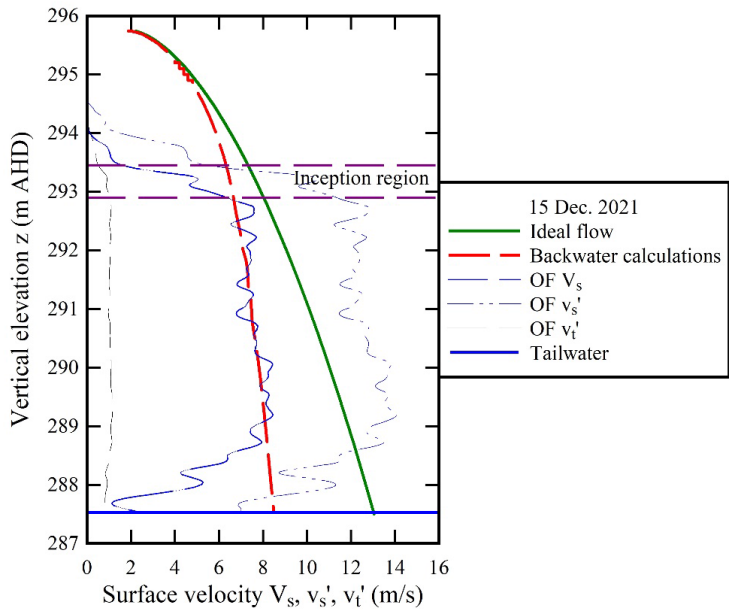(B) On 15 December 2022 (Q = 144 m³/s)

Fig. 8 Time-averaged OF surface velocity: comparison between time-averaged optical flow (OF) surface velocity data, ideal fluid flow velocity and backwater calculations at Chinchilla MEL weir

Fig. 9 Contour map of time-averaged surface velocity and standard deviation of longitudinal velocity ▶
at Chinchilla (MEL) weir on 27 November 2021—Location: middle of left spillway bay, Time: 14:18,
Number of analysed frames: 840, Resolution: 0.00515 m/px, Frame rate: 30 fps. **A** Time-averaged
longitudinal surface velocity. **B** Standard deviation of longitudinal surface velocity

The comparison reflects well the adequacy of the backwater calculations assuming a
gradually-varied chute flow. While the method was herein applied to the self-aerated
flow region, drag reduction caused by self-aeration was not expected to occur for this flat
slope (1 V:5H), because of the small values of mean void fraction down the chute slope,
with nil to negligible effect on the friction factor, even if quasi uniform air–water flow
would be attained (e.g. as per [12]. At the downstream end of the chute, i.e. for $z_o < 288$ m
AHD, a lack of match with backwater estimate might be caused by optical artifacts caused
by spray and splashing above the hydraulic jump roller at the chute toe. Indeed, visual
observations by the first author showed drops and splash reaching heights of more than
0.5–1 m above the hydraulic jump roller surface. Fourthly, the OF data output quality was
closely linked to the quality of the original movies. Practical considerations encompassed
the camera position, ideally placed perpendicularly to the spillway chute, a sturdy camera
tripod, and the camera body and lens equipment, with all the present data set acquired with
professional-grade full-frame prime lenses, following earlier experiences [6, 19, 21]. More,
a higher movie definition delivered improved outputs with greater spatial resolutions, i.e.
less millimetres per pixel. It is worth to mention that both OF field data sets were filmed
under good weather conditions, hence decent lighting conditions.

5.2 Surface velocity field in the self-aerated flow region

The OF surface velocity characteristics were analysed in the self-aerated flow region, in
terms of the contour maps of time-averaged longitudinal velocity component, standard
deviations of the longitudinal and transverse surface velocity. Typical contour maps of
the time-averaged longitudinal velocity component V_s and standard deviations v_s' of the
longitudinal surface velocity are shown in Figs. 9 and 10. In Figs. 9 and 10, the horizontal
axis is a transverse coordinate, the vertical axis is the vertical elevation in m AHD, and the
contour data are the velocity data measured parallel to the invert. The legend on the right
of Figs. 9 and 10 explains the colour coding of the contour maps. In the contour maps, the
tailwater level is shown as well.

As seen in Figs. 8, 9 and 10, the results were unreliable in the upstream non-aerated
flow. Further, the surface velocity data were not reliable below elevation 288 m AHD,
because of the splashing above the hydraulic jump roller. In the self-aerated flow region,
the surface velocity data implied some regions of high-velocity and others of low-veloc-
ity. That is, longitudinal "canyons" of faster flowing water, with streaks of lower surface
velocities in between, in the self-aerated flow region downstream of the inception region.
The same data sets highlighted regions of high- and low-streamwise velocity fluctuations.
The observations were similar to recent field observations at the Hinze Dam Stage 3 [19,
21] and in a relatively large-size spillway model [6]. The findings are important in terms of
the design and operation of energy dissipators, e.g. hydraulic jump stilling basins and ski
jumps. Indeed, these regions of high velocity are associated with concentrations in kinetic
energy that must be dissipated safely in the stilling structure.

Further, the weighted averages of the velocity standard deviations are presented
in Table 4, together with the number of analysed frames, the frame rate and the spatial
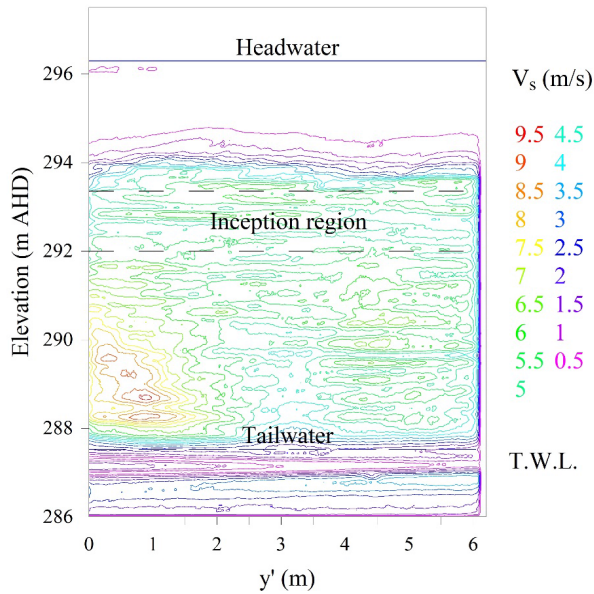
(A) Time-averaged longitudinal surface velocity
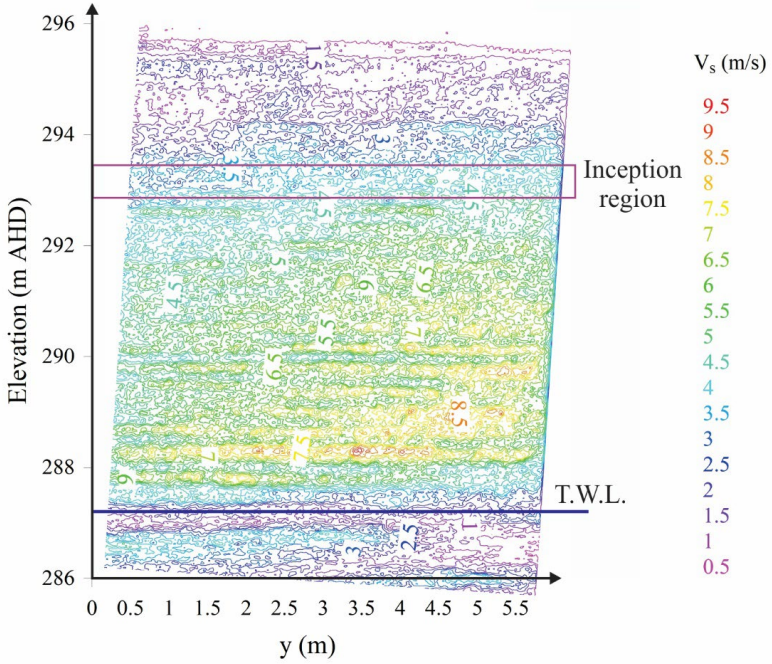
(B) Standard deviation of longitudinal surface velocity
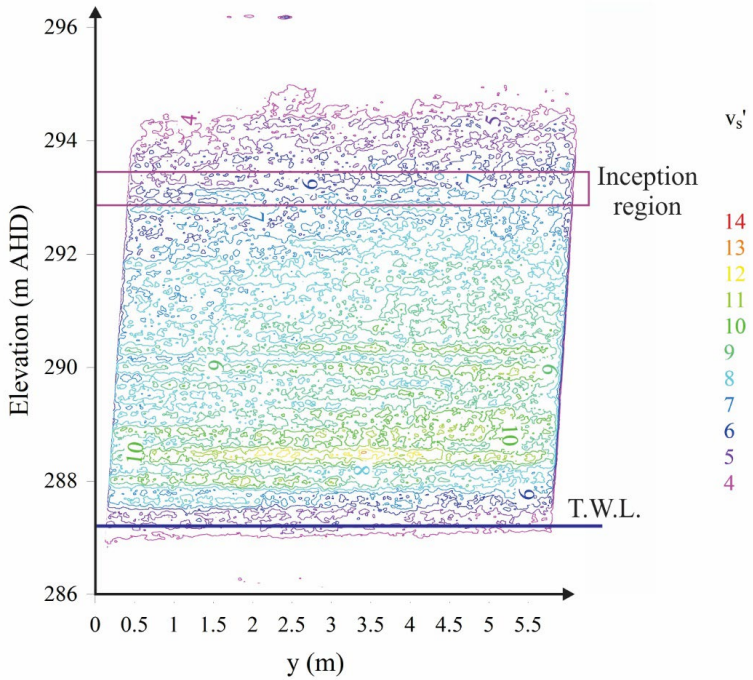
(A) Time-averaged longitudinal surface velocity

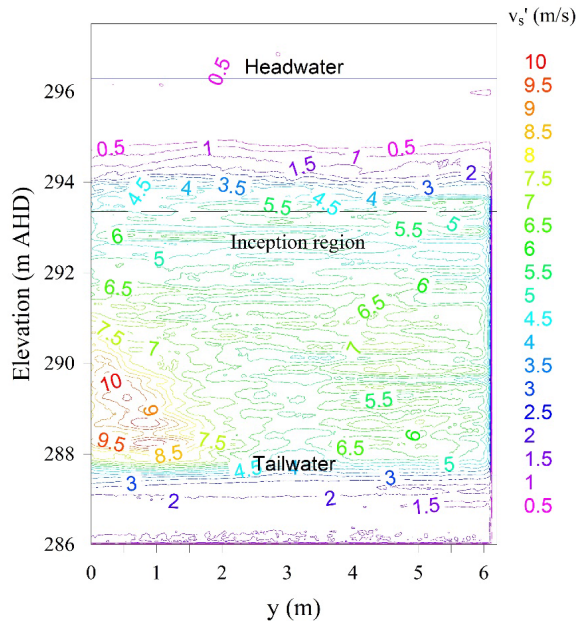(B) Standard deviation of longitudinal surface velocity

Fig. 10 Contour map of time-averaged surface velocity and standard deviation of longitudinal velocity at Chinchilla (MEL) weir on 15 December 2021—Location: middle of left spillway bay, Time: 12:31, Number of analysed frames: 18,090, Resolution: 0.00579 m/px, Frame rate: 60 fps. **A** Time-averaged longitudinal surface velocity. **B** Standard deviation of longitudinal surface velocity

Table 4 Surface turbulence properties in the self-aerated flow at Chinchilla MEL weir (QLD, Australia) during the Nov./Dec. 2011 flood event

Date	Q (m^3/s)	Frame rate (fps)	Total Nb of analysed frames	Spatial resolution (mm/px)	v_s'/V_s ([1]) ([2]) ([3])	v_t'/V_s ([1]) ([2]) ([3])	v_t'/v_s' ([1]) ([2]) ([3])
27 November 2021	121	30 & 60	6,660	5.15 & 7.2	1.71	0.111	0.064
15 December 2021	144	30 & 60	92,310	5.8 & 8.3	2.09	0.165	0.096

V_s: time-averaged longitudinal surface velocity; v_s': standard deviation of longitudinal surface velocity; v_t': standard deviation of transverse surface velocity; ([1]) weighted average for all analysed movies; ([2]) analyses of image centreline; ([3]) observations for 288 m AHD $< z_o <$ 293 m AHD

resolutions. Noteworthy, the data are based upon a large number of analysed frames in the current study (Table 4, 4th column). The streamwise velocity data presented large surface turbulent intensity $Tu_s = v_s'/V_s$ in the range 1.7 to 2 (Table 4, 6th column). The large values were likely the resulting combination of (a) relatively large velocity fluctuations initiated by surface wave motion and of (b) true turbulence. The data were quantitatively of the same magnitude as a series of field measurements at the Hinze Dam spillway [20] and as self-aerated flow data in large-size laboratory facilities [6, 23]. In contrast, the transverse velocity data exhibited much lower transverse surface turbulent intensity $Tu_t = v_t'/V_s$ within 0.11–0.17, likely induced by the smooth convergence of the flow. The ratio Tu_t/Tu_s was between 0.06 and 0.1 (Table 4, 8th column). Such a result implied some very strong anisotropy of the surface turbulence. Noteworthy, the present prototype observations were close to reported values of the ratio v_t'/v_s' in rough turbulent boundary layers [51] and on the Hinze Dam prototype spillway [21].

6 Discussion

The present study results may be compared to earlier results in free-surface investigations in prototype and laboratory spillways, although most were conducted with steep stepped spillways (Table 5). All the observations showed that the onset of self-aeration extended over a surface plane with some transient pattern, constantly fluctuating about a mean location. On the smooth relatively flat spillway of Chinchilla weir, the longitudinal transition from non-aerated to air–water flow region was somewhat gradual, while it was sudden and violent on steep stepped chutes. On steep stepped spillways, the onset was driven by the interactions of the developing boundary layer turbulence with the free-surface [10, 21, 45, 58]. At Chinchilla MEL weir, it is believed that the inception of self-aeration resulted from the combined interactions between surface instabilities and developing boundary layer.

The surface velocity data showed marked differences in the applicability of the OF calculation. Physically meaningful results were achieved in terms of the self-aerated surface velocity field in the large-size stepped spillway model and Chinchilla MEL weir spillway (Table 5). In both cases, the motion of the "grainy" air–water surface roughness was successfully captured by the OF method. Several studies discuss the influence of surface roughness on the inception of self-aeration (e.g. [7, 8, 56], while the interactions between self-aeration and surface waves were shown to have relatively little influence on the void fraction and air entrainment rate [53]. On prototype stepped spillways (Table 5), the air–water region exhibited an intensely bright white colour which prevented any detection of structure advection, with the camera equipment used in these studies, although it is conceivable that IR camera systems might be more successful.

Finally, it is acknowledged that the OF data were obtained with relatively low frame rates, compared to recent laboratory studies [6, 9, 59]. Indeed, the application of OF technique differs substantially between laboratory and field [19, 20], and its implementation for prototype flow tends to be closer to large-sale particle image and infrared quantitative image velocimetry applications (e.g. [38, 39, 52]). There are however some key differences between laboratory and field applications of OF, linked to the differences in light intensity often limited indoors, surface feature sizes typically smaller in laboratory, and location of camera often restricted in the field. While ideally a faster frame rate would be desirable,

Table 5 Free-surface investigations in prototype spillways and large-size laboratory model

Spillway	Spillway type	Invert slope θ (°)	Investigation year(s)	OF spatial resolution (mm/px)	Image size (px)	Frame rate (fps)	Reference
Chinchilla MEL weir	Smooth chute	11.3	2021	5.15 to 8.3	1920×1080	30 & 60	Present
Paradise Dam	Stepped spillway (h = 0.62 m)	57.4[1]	2010 & 2013	N/A	N/A	N/A	Chanson et al. [18, 19, 22]
Hinze Dam Stage 3	Stepped spillway (h = 1.5 m)	51.3[1]	2013, 2015, 2017, 2021, 2022	10.5 to 42.4	1920×1080	30 & 60	Chanson [16, 19–21]
UQ spillway model[2]	Stepped spillway (h = 0.1 m)	45	2020–2021	0.51 & 0.87[2]	1280×800	22,000	Arosquipa Nina et al. [6]

[1] At end of ogee development

[2] Top view observations

other practical considerations tend to be more important and relevant to ensure successful surface velocity data in prototype spillway [20].

7 Conclusion

The Minimum Energy Loss (MEL) weir design was developed in Queensland, Australia specifically for the river catchments affected by heavy tropical and sub-tropical rainfalls where streams have very flat gradients and erodible banks. A number of MEL weirs have successfully operated for many decades and the operations of two of them were discussed. Inspections during and after major flood events indicated a reliable operation associated with minimum maintenance. The historical performances of the MEL weirs have confirmed the design capability to pass large floods with small afflux and very small energy loss and that they cause no significant erosion at their abutments or downstream—the regions that are most at risk and require extensive protection for conventional weirs.

During the November-December 2021 flood, visual and quantitative observations were undertaken at the Chinchilla MEL weir. The spillway chute was observed and documented during two days, at the start and towards the end of a major flood event peaking on 5 December 2021. The approach flow was very smooth and streamlined before it reached the broad crest, and then continued down a converging smooth chute. Downstream of the crest, the chute flow presented a very smooth and glassy free-surface. On 17 November 2021, the presence of large logs, blocked on the crest, had no major impact on the chute flow. Further downstream on the smooth converging chute, the observations showed that the inception of self-aeration was a three-dimensional process with a 'progressive' change in free-surface roughness, from a smooth glassy free-surface, to a coarse-sand-paper-like appearance and then a very-rough choppy surface. Both the upstream non-aerated and self-aerated flow regions exhibited a brown colour indicating the large amount of suspended sediment materials.

An optical technique was implemented to derive the contour maps of surface velocities based upon video movies taken from a sturdy tripod. The present data sets showed results close to the backwater equation in the self-aerated region, while highlighting large transverse difference in longitudinal surface velocities across the chute. The OF data presented large streamwise surface velocity fluctuations in the aerated flow region, with $Tu_s \sim 150$–200%, consistent with other field data sets and some literature on self-aerated flow measurements using dual-tip phase detection probe in large-size laboratory models. The ratio of transverse to streamwise surface turbulence intensity Tu_t / Tu_s was between 0.06 and 0.1, indicating a strong anisotropy of the free-surface turbulence.

Data availability Some or all data, or models that support the findings of this study are available from the corresponding author upon reasonable request.

Declarations

Conflict of interest Hubert Chanson has a major conflict of interest with Matthias Kramer.

References

1. Anwar HO (1994) Self-aerated flows on chutes and spillways: discussion. J Hydraul Eng ASCE 120(6):778–779
2. Apelt CJ (1978) A commemorative volume presented to Professor Gordon R. McKay on the Occasion of his Retirement from the Department of Civil Engineering of The University of Queensland. 20th December 1978. Manuscript, Dept of Civil Engrg., Univ. of Queensland, Brisbane, Australia, p 82
3. Apelt CJ (1983) Hydraulics of minimum energy culverts and bridge waterways. Aust Civ Eng Trans 25(2):89–95
4. Apelt CJ (2002) What has Fluid Mechanics got to do with it? Aust J Water Resour Inst Eng Aust 5(2):123–136. https://doi.org/10.1080/13241583.2002.11465199
5. Apelt CJ, Chanson (2022) Hydraulics of minimum energy loss weir: the Chinchilla MEL weir during the Nov–Dec 2021 flood event. In: Proc. hydrology and water resources symposium HWRS2022, Engineers Australia, 30 Nov–2 Dec, Brisbane, Australia. Paper 09, pp 64–75
6. Arosquipa Nina Y, Shi R, Wűthrich D, Chanson H (2022) Intrusive and non-intrusive two-phase air-water measurements on stepped spillways: a physical study. Exp Therm Fluid Sci 131(110545):22. https://doi.org/10.1016/j.expthermflusci.2021.110545
7. Brocchini M, Peregrine DH (2001) The dynamics of strong turbulence at free surfaces. part 1. Description. J Fluid Mech 449:225–254
8. Bung DB (2013) Non-intrusive detection of air–water surface roughness in self-aerated chute flows. J Hydraul Res IAHR 51(3):322–329. https://doi.org/10.1080/00221686.2013.777373
9. Bung DB, Valero D (2016) Optical flow estimation in aerated flows. J Hydraul Res IAHR 54(5):575–580. https://doi.org/10.1080/00221686.2016.1173600
10. Cain P, Wood IR (1981) Measurements of self-aerated flow on a spillway. J Hydraul Div ASCE 107(HY11):1425–1444
11. Chanson H (1997) Air bubble entrainment in open channels. Flow structure and bubble size distributions. Int J Multiph Flow 23(1):193–203. https://doi.org/10.1016/S0301-9322(96)00063-8
12. Chanson H (1997) Air bubble entrainment in free-surface turbulent shear flows. Academic Press, London, p 401
13. Chanson H (2001) The hydraulics of stepped chutes and spillways. Balkema, Lisse
14. Chanson H (2003) Minimum energy loss structures in australia: historical development and experience. In: Proc. 12th national engineering heritage conference, IEAust., Toowoomba Qld, Australia, N. Sheridan Ed., pp 22–28

15. Chanson H (2004) The hydraulics of open channel flow: an introduction, 2nd edn. Butterworth-Heinemann, Oxford, p 630
16. Chanson H (2013) Interactions between a developing boundary layer and the free-surface on a stepped spillway: hinze dam spillway operation in January 2013. In: Proceeding 8th international conference on multiphase flow ICMF 2013, Jeju, Korea, 26–31 May, Gallery Session ICMF2013–005 (Video duration: 2:15). https://www.youtube.com/watch?v=cKHDrkNFfC0&t=3s
17. Chanson H (2014) Applied hydrodynamics: an introduction. CRC Press, Taylor & Francis Group, Leiden, p 448
18. Chanson H (2015) Embankment overtopping protection systems. Acta Geotecnica 10(3):305–318. https://doi.org/10.1007/s11440-014-0362-8
19. Chanson H (2021) Stepped spillway prototype operation, spillway flow and air entrainment: the Hinze Dam, Australia. Hydraulic Model Report No. CH123/21, School of Civil Engineering, The University of Queensland, Brisbane, Australia, p 183. https://doi.org/10.14264/c8d5280
20. Chanson H (2022) On air entrainment onset and surface velocity in high-speed turbulent prototype flows. Flow Meas Instrum 83:102122. https://doi.org/10.1016/j.flowmeasinst.2022.102122
21. Chanson H (2022) Stepped spillway prototype operation and air entrainment: toward a better understanding of the mechanisms leading to air entrainment in skimming flows. J Hydraul Eng ASCE 148(11):05022004. https://doi.org/10.1061/(ASCE)HY.1943-7900.0002015
22. Chanson H, Bung D, Matos J (2015) Stepped spillways and cascades. In: Energy dissipation in hydraulic structures. IAHR Monograph, CRC Press, Taylor & Francis Group, Leiden, The Netherlands, H. Chanson Editor, pp 45–64
23. Chanson H, Toombes L (2002) Air-water flows down stepped chutes: turbulence and flow structure observations. Int J Multiph Flow 28(11):1737–1761. https://doi.org/10.1016/S0301-9322(02)00089-7
24. Chow VT (1973) Open channel hydraulics. McGraw-Hill International, New York
25. Dressler RF (1949) Mathematical solution of the problem of roll-waves in inclined open channels. Commun Pure Appl Phys 2(2–3):149–194
26. Farnebäck G (2003) Two-frame motion estimation based on polynomial expansion. In: Proc. Scandinavian conference on Image analysis. Springer, Berlin, Heidelberg, pp 363–370
27. FEMA (2014) Overtopping protection for dams. Technical Manual P-1015, US Bureau of Reclamation, p 462
28. Gordienko PI (1978) Reinforced-concrete-earth overflow dams. Dams & Spillways, Collection of Works No. 61, Issue 2, MISI, Moscow, pp 3–17 (**in Russian**)
29. Halbronn G (1952) "Etude de la Mise en Régime des Ecoulements sur les Ouvrages à Forte Pente. Applications au Problème de l'Entraînement d'Air." Journal La Houille Blanche, No. 1, pp. 21–40; No. 3, pp. 347–371; No. 5, pp. 702–722 (**in French**)
30. Halbronn G, Durand R, Cohen de Lara G (1953) Air Entrainment in Steeply Sloping Flumes. In: Proc. 5th IAHR Congress, IAHR-ASCE, Minneapolis, USA, pp 455–466
31. Hino M (1961) A theory of the mechanism of self-aerated flow on steep slope channels. Applications of the Statistical Theory of Turbulence. Technical Report C-6101, Technical Laboratory, Central Research Institute of Electric Power Industry, Japan, p 42
32. Ippen AT, Tankin RS, Raichekn F (1955) Turbulence measurements in free- surface flow with an impact tube-pressure transducer combination. Technical Report No. 20, MIT, Department of Civil and Sanitary Engineering, p 112
33. Irrigation and Water Supply Commission (1972) "Chinchilla weir layout. As constructed." Drawing L44375 75313, Version B, 16/5/1972
34. Keller RJ, Rastogi AK (1975) Prediction of flow development on spillways. J Hydraul Div ASCE 101(HY9):1171–1184
35. Keulegan GH, Patterson GW (1940) A criterion for instability of flow in steep channels. Trans Am Geophys Union Pt II 21:594–596
36. Lane EW (1936) Recent studies on flow conditions in steep chutes. Eng News-Rec 2:5–7
37. Lane EW (1939) Entrainment of air in swiftly flowing water. Observations of the flow over spillways yield conclusions of interest to hydraulic engineers. Civ Eng 2:89–91
38. Le Boursicaud R, Penard L, Hauet A, Thollet F, Le Coz J (2016) Gauging extreme floods on YouTube: application of LSPIV to home movies for the post-event determination of stream discharges. Hydrol Process 30:90–105
39. Le Coz J, Renard B, Vansuyt V, Hauet A, Jodeau M (2020) Video-based hydrometry: a Bayesian camera calibration method for uncertainty analysis. In: Proceedings of RiverFlow2020, CRC Press, Uijttewaal, 2020, pp 1053–1060
40. Levi E (1965) Longitudinal streaking in liquid currents. J Hydraul Res IAHR 3(2):25–39

41. Levi E (1967) "Macroturbulence Produced by Vortex Breakdown in High Velocity Flows." Proc. 12th IAHR Congress, Colorado, USA, Vol. 2. Paper B7:54–60
42. Liggett JA (1994) Fluid mechanics. McGraw-Hill, New York
43. McKay GR (1971) Design of minimum energy culverts. Research Report, Dept of Civil Eng., University of Queensland, Brisbane, Australia, p 29
44. McLean FG, Hansen KD (1993) Roller compacted concrete for embankment overtopping protection. In: Proc. Spec. Conf. on Geotechnical Practice in Dam Rehabilitation, ASCE, Raleigh NC, USA, L.R. Anderson editor, pp 188–209
45. Meireles IC, Bombardelli FA, Matos J (2014) Air entrainment onset in skimming flows on steep stepped spillways: an analysis. J Hydraul Res IAHR 52(3):375–385. https://doi.org/10.1080/00221686.2013.878401
46. Michels V, Lovely M (1953) Some prototype observations of air entrained flow. In: Proc. 5th IAHR Congress, IAHR-ASCE, Minneapolis, USA, pp 403–414
47. Montes JS (1998) Hydraulics of open channel flow. ASCE Press, New-York, p 697
48. Pravdivets YP (1987) Industrial design of an earth overflow dam. Gidrotekhnicheskoe Stroitel'stvo 12:15–18 (**in Russian**)
49. Queensland Government (1970) Report on Weir on Condamine River at Chinchilla for Dual Purpose. Town and Irrigation Water Supply. Department of Local Government, Queensland Irrigation and Water Supply Commission, Brisbane, Australia, Feb., 18 pages & 2 Drawings
50. Rao NSG, Rajaratnam N (1961) On the inception of air entrainment in open channel flows. In: Proc. 9th IAHR Congress, Dubrovnick, Yugoslavia, pp 9–12
51. Schlichting H, Gersten K (2000) Boundary layer theory, 8th edn. Springer, Berlin, p 707
52. Schweitzer SA, Cowen EA (2021) Instantaneous riverwide water surface velocity field measurements at centimeter scales using infrared quantitative image velocimetry. Water Resources Res AGU 57:e2020WR029279. https://doi.org/10.1029/2020WR029279
53. Toombes L, Chanson H (2007) Surface waves and roughness in self-aerated supercritical flow. Environ Fluid Mech 7(3):259–270. https://doi.org/10.1007/s10652-007-9022-y
54. Toro JP, Bombardelli FA, Paik J (2017) Detached eddy simulation of the nonaerated skimming flow over a stepped spillway. J Hydraul Eng ASCE 143(9):04017032
55. Turnbull JD, McKay GR (1974) The Design and Construction of Chinchilla Weir - Condamine River Queensland." Proc. 5th Australasian Conf. on Hydraulics and Fluid Mechanics. Christchurch, New Zealand II:1–8
56. Valero D, Bung DB (2016) Development of the interfacial air layer in the non-aerated region of high-velocity spillway flows. Instabilities growth, entrapped air and influence on the self-aeration onset. Int J Multiph Flow 84:66–74
57. Zabaleta F, Bombardelli FA (2020) Eddy-resolving simulation of flows over macroroughness. In: Proceedings of RiverFlow2020, CRC Press, Uijttewaal et al. Editors, pp 1293–1299
58. Zhang G, Chanson H (2016) Hydraulics of the developing flow region of stepped spillways: I: physical modeling and boundary layer development. J Hydraul Eng ASCE 142(7):8. https://doi.org/10.1061/(ASCE)HY.1943-7900.0001138
59. Zhang G, Chanson H (2018) Application of local optical flow methods to high-velocity free-surface flows: validation and application to stepped chutes. Exp Thermal Fluid Sci 90:186–199. https://doi.org/10.1016/j.expthermflusci.2017.09.010